symmetry

IMPACT FACTOR 2.7

CITESCORE 4.9

Article

Quantum-Number Projected Generator Coordinate Method for ^{21}Ne with a Chiral Two-Nucleon-Plus-Three-Nucleon Interaction

Wei Lin, Enfu Zhou, Jiangming Yao and Heiko Hergert

Special Issue

Restoration of Broken Symmetries in the Nuclear Many-Body Problem

Edited by

Prof. Dr. Javid Sheikh and Prof. Dr. Peter Ring

MDPI

https://doi.org/10.3390/sym16040409

symmetry

MDPI

Article

Quantum-Number Projected Generator Coordinate Method for ^{21}Ne with a Chiral Two-Nucleon-Plus-Three-Nucleon Interaction

Wei Lin [1], Enfu Zhou [1], Jiangming Yao [1,*] and Heiko Hergert [2,3]

[1] School of Physics and Astronomy, Sun Yat-sen University, Zhuhai 519082, China; linw33@mail2.sysu.edu.cn (W.L.); zhouenf@mail2.sysu.edu.cn (E.Z.)
[2] Facility for Rare Isotope Beams, Michigan State University, East Lansing, MI 48824-1321, USA; hergert@nscl.msu.edu
[3] Department of Physics & Astronomy, Michigan State University, East Lansing, MI 48824-1321, USA
* Correspondence: yaojm8@sysu.edu.cn

Abstract: In this paper, we report a study of the low-lying states of deformed ^{21}Ne within the framework of the quantum-number projected generator coordinate method (PGCM), starting from a chiral two-nucleon-plus-three-nucleon ($NN+3N$) interaction. The wave functions of states are constructed as a linear combination of a set of axially deformed Hartree–Fock–Bogliubov (HFB) wave functions with different quadrupole deformations. These HFB wave functions are projected onto different angular momenta and the correct neutron and proton numbers for ^{21}Ne. The results of the calculations based on the effective Hamiltonians derived by normal-ordering the $3N$ interaction with respect to three different reference states, including the quantum-number projected HFB wave functions for ^{20}Ne, ^{22}Ne, and an ensemble of them with equal weights, are compared. This study serves as a key step towards ab initio calculations of odd-mass deformed nuclei with the in-medium GCM.

Keywords: symmetry restoration; generator coordinate method; nuclear chiral interaction; odd-mass nuclei; quadrupole deformation

Citation: Lin, W.; Zhou, E.; Yao, J.; Hergert, H. Quantum-Number Projected Generator Coordinate Method for ^{21}Ne with a Chiral Two-Nucleon-Plus-Three-Nucleon Interaction. *Symmetry* **2024**, *16*, 409. https://doi.org/10.3390/sym16040409

Academic Editor: Angel Gómez Nicola

Received: 2 March 2024
Revised: 25 March 2024
Accepted: 27 March 2024
Published: 1 April 2024

1. Introduction

Studying nuclear low-lying states, including energy spectra and electroweak transition strengths, is crucial for advancing our understanding of nuclear physics [1,2]. It also plays a key role in exploring new physics at the high-precision frontier, such as nonzero electric dipole moments [3,4], single-β decay [5], and neutrinoless double-β decay [6]. Modeling the low-lying states of light to heavy atomic nuclei directly from the fundamental interactions between nucleons is of great interest for this purpose. Compared to even-even nuclei, the low-lying states of odd-mass nuclei contain richer nuclear structure information because of the interplay of single-particle and collective motions, presenting a considerable challenge for nuclear theory.

The generator coordinate method (GCM) provides an efficient and flexible framework to describe the wave function of a quantum many-body system, represented as a superposition of a set of nonorthogonal basis functions, such as Slater determinants, generated by continuously changing parameters called generator coordinates [7,8]. In nuclear physics, the quantum-number projected GCM (PGCM) has been extensively employed in studies of the energies and transition rates of low-lying states. See, for instance, refs. [9–11]. In the recent decade, the PGCM has been implemented into ab initio methods for atomic nuclei. This idea has given birth to a new generation of ab initio methods, including the no-core Monte Carlo shell model [12], the in-medium generator coordinate method (IM-GCM) [13,14] and perturbative PGCM with second-order perturbation theory, abbreviated as PGCM-PT(2) [15–17].

In this paper, we extend the PGCM for the low-lying states of an odd-mass deformed nucleus ^{21}Ne, starting from a Hamiltonian composed of two-plus-three-nucleon ($NN+3N$)

interaction derived from chiral effective field theory (EFT). The PGCM has been extended for odd-mass nuclei based on different energy density functionals (EDFs) [18–26]. It is known that EDF-based PGCM approaches may suffer from spurious divergences and discontinuities [26–29]. In this work, we examine that this Hamiltonian-based framework is free of those problems as the same interaction is applied to both the particle-hole and particle-particle channels when computing the energy overlaps of Hamiltonian kernels. Additionally, we compare the energy spectra of the low-lying states from the PGCM calculations using the effective Hamiltonian normal-ordered with respect to the following three different reference states: ^{20}Ne, ^{22}Ne, and an ensemble with equal weights.

The article is arranged as follows: in Section 2, we present the main formulas of PGCM for an odd-mass nucleus, including the generation of an effective Hamiltonian in the normal-ordering two-body (NO2B) approximation, and the construction of nuclear wave functions in the PGCM. The results of calculations for ^{21}Ne are presented in Section 3. A short summary and outlook are provided in Section 4.

2. The PGCM for an Odd-Mass Nucleus

2.1. Nuclear Hamiltonian

We employ an intrinsic nuclear A-body Hamiltonian containing both NN and $3N$ interactions,

$$\hat{H}_0 = \left(1 - \frac{1}{A}\right) T^{[1]} + \frac{1}{A} T^{[2]} + \sum_{i<j} V_{ij}^{[2]} + \sum_{i<j<k} W_{ijk}^{[3]}, \tag{1}$$

where the kinetic term is composed of one- and two-body terms,

$$T^{[1]} = \sum_{i=1}^{A} \frac{\mathbf{p}_i^2}{2m_N}, \quad T^{[2]} = -\sum_{i<j} \frac{\mathbf{p}_i \cdot \mathbf{p}_j}{m_N}, \tag{2}$$

with m_N being the mass of nucleon and $\mathbf{p}_i$ the momentum of the i-th nucleon.

The above Hamiltonian is normal-ordered with respect to a symmetry-conserving reference state $|\Psi\rangle$, and truncated up to NO2B terms. The resultant Hamiltonian $\hat{\mathcal{H}}_0$ in the NO2B approximation can be written as

$$\hat{\mathcal{H}}_0 = E_0 + \sum_{pq} f_q^p :A_q^p: + \frac{1}{4} \sum_{pqrs} \Gamma_{rs}^{pq} :A_{rs}^{pq}:, \tag{3}$$

where the strings of creation and annihilation operators are defined as

$$A_{stu\ldots}^{pqr\ldots} = a_p^\dagger a_q^\dagger a_r^\dagger \ldots a_u a_t a_s. \tag{4}$$

The expectation values of the normal-ordered operators, indicated by $:A_{q\ldots}^{p\ldots}:$, with respect to the reference state are zero. The zero-body piece of the $\mathcal{H}_0$ is just the energy of the reference state

$$E_0 \equiv \langle \Psi | \hat{H}_0 | \Psi \rangle = \sum_{pq} \bar{t}_q^p \gamma_q^p + \frac{1}{4} \sum_{pqrs} \bar{v}_{rs}^{pq} \gamma_{rs}^{pq} + \frac{1}{36} \sum_{pqrstu} w_{stu}^{pqr} \gamma_{stu}^{pqr}, \tag{5}$$

where the matrix element of the normal-ordered one-body operator (NO1B) is given by

$$f_q^p = \bar{t}_q^p + \sum_{rs} \bar{v}_{rs}^{pq} \gamma_s^r + \frac{1}{4} \sum_{rstu} w_{qtu}^{prs} \gamma_{tu}^{rs}, \tag{6}$$

and that of the NO2B operator,

$$\Gamma_{rs}^{pq} = \bar{v}_{rs}^{pq} + \sum_{tu} w_{rsu}^{pqt} \gamma_u^t. \tag{7}$$

In the above equations, the symbols hatted with bars are introduced for the sake of brevity,

$$\bar{t} \equiv \left(1 - \frac{1}{A}\right) T^{[1]}, \quad \bar{v} \equiv \frac{1}{A} T^{[2]} + V^{[2]}, \quad w \equiv W^{[3]}. \tag{8}$$

The last terms in (5)–(7) contributed by the 3N interaction are depicted schematically in Figure 1a–c, respectively. Here, we have introduced the density matrices of the (symmetry-conserving) correlated reference state $|\Psi\rangle$,

$$\gamma^p_q \equiv \langle\Psi| A^p_q |\Psi\rangle , \tag{9a}$$
$$\gamma^{pq}_{rs} \equiv \langle\Psi| A^{pq}_{rs} |\Psi\rangle , \tag{9b}$$
$$\gamma^{pqr}_{stu} \equiv \langle\Psi| A^{pqr}_{stu} |\Psi\rangle . \tag{9c}$$

Static correlations within the reference state are encoded in the corresponding *irreducible* density matrices

$$\lambda^p_q \equiv \gamma^p_q , \tag{10a}$$
$$\lambda^{pq}_{rs} \equiv \gamma^{pq}_{rs} - \mathcal{A}(\lambda^p_r \lambda^q_s) = \gamma^{pq}_{rs} - \lambda^p_r \lambda^q_s + \lambda^p_s \lambda^q_r , \tag{10b}$$
$$\lambda^{pqr}_{stu} \equiv \gamma^{pqr}_{stu} - \mathcal{A}(\lambda^p_s \lambda^{qr}_{tu} + \lambda^p_s \lambda^q_t \lambda^r_u) , \tag{10c}$$

where the antisymmetrization operator $\mathcal{A}$ generates all possible permutations (each only once) of upper indices and lower indices. For a single-reference state, the two-body and three-body irreducible densities λ^{pq}_{rs} and λ^{pqr}_{stu} vanish. The expressions for the one-, two-, and three-body irreducible density matrices of a particle-number projected spherical HFB wave function have been given in Ref. [30].

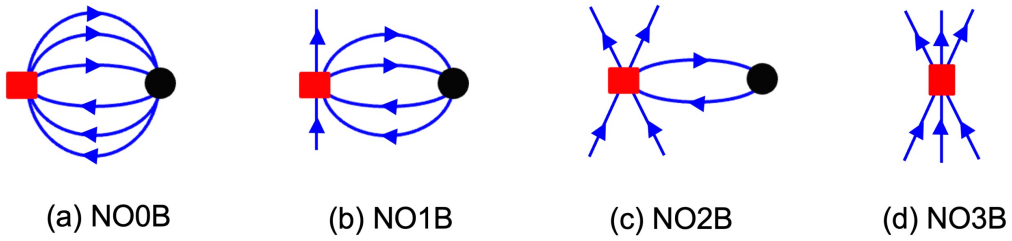

Figure 1. Schematic illustration of the three-nucleon interaction W (red squares), normal-ordered to (**a**) zero-body, (**b**) one-body, (**c**) two-body, and (**d**) three-body terms with a reference state. The density matrices γ of the reference state are represented with black circles.

The Hamiltonian $\hat{\mathcal{H}}_0$ is subsequently rewritten into the unnormal-ordered form as follows:

$$\hat{\mathcal{H}}_0 = \mathscr{E}_0 + \sum_{pq} \mathscr{F}^p_q A^p_q + \frac{1}{4} \sum_{pqrs} \mathscr{V}^{pq}_{rs} A^{pq}_{rs}, \tag{11}$$

where the zero-body term is given by

$$\begin{aligned} \mathscr{E}_0 &= E_0 - \sum_{pq} \left(f^p_q - \sum_{rs} \Gamma^{pr}_{qs} \gamma^r_s \right) \gamma^p_q - \frac{1}{4} \sum_{pqrs} \Gamma^{pr}_{qs} \gamma^{pr}_{qs} \\ &= \frac{1}{36} \sum_{pqrstu} w^{pqr}_{stu} \left(\gamma^{pqr}_{stu} + 36 \gamma^p_s \gamma^q_t \gamma^r_u - 18 \gamma^{pq}_{st} \gamma^r_u \right) \\ &= \frac{1}{36} \sum_{pqrstu} w^{pqr}_{stu} \left(6 \lambda^p_s \lambda^q_t \lambda^r_u - 9 \lambda^{pq}_{st} \lambda^r_u + \lambda^{pqr}_{stu} \right). \end{aligned} \tag{12}$$

The matrix elements of one-body read

$$\begin{aligned} \mathscr{F}_q^p &= f_q^p - \sum_{rs} \Gamma_{qs}^{pr} \gamma_s^r \\ &= \bar{t}_q^p + \frac{1}{4} \sum_{rstu} w_{qtu}^{prs} \left(\lambda_{tu}^{rs} - 2\lambda_t^r \lambda_u^s \right), \end{aligned} \tag{13}$$

and those of two-body terms

$$\mathscr{V}_{rs}^{pq} = \Gamma_{rs}^{pq} = \bar{v}_{rs}^{pq} + \sum_{tu} w_{rstu}^{pqt} \lambda_u^t. \tag{14}$$

In this work, the reference state is chosen as a particle-number projected HFB state for ^{20}Ne and ^{22}Ne, which are labeled with `magic-Ne20` and `magic-Ne22`, respectively. The obtained effective Hamiltonians $\mathcal{H}_0$ are labeled as `H0`. For comparison, we also derive the Hamiltonian without the 3N interaction term in (1), and this Hamiltonian is labeled as `H0 (w/o 3N)`. The expressions for the one-, two-, and three-body density matrices of the particle-number projected HFB state have been given in Ref. [30]. Subsequently, these Hamiltonians are employed into the PGCM calculations.

2.2. Nuclear Wave Functions

The wave functions of low-lying states for an odd-mass nucleus are constructed with the PGCM as follows:

$$|\Psi_\alpha^{J\pi}\rangle = \sum_c f_c^{J\alpha\pi} |NZJ\pi; c\rangle, \tag{15}$$

where α distinguishes the states with the same angular momentum J, and the symbol c is a collective label for the indices $(K, \kappa, \mathbf{q})$. The basis function with correct quantum numbers $(NZJ\pi)$ is given by

$$|NZJ\pi; c\rangle = \hat{P}_{MK}^J \hat{P}^N \hat{P}^Z |\Phi_\kappa^{(\mathrm{OA})}(\mathbf{q})\rangle, \tag{16}$$

where $\hat{P}_{MK}^J$ and $\hat{P}^{N,Z}$ are projection operators that select components with the angular momentum J, neutron number N, and proton number Z [2],

$$\hat{P}_{MK}^J = \frac{2J+1}{8\pi^2} \int d\Omega D_{MK}^{J*}(\Omega) \hat{R}(\Omega), \tag{17a}$$

$$\hat{P}^{N_\tau} = \frac{1}{2\pi} \int_0^{2\pi} d\varphi_\tau e^{i\varphi_\tau(\hat{N}_\tau - N_\tau)}. \tag{17b}$$

The operator $\hat{P}_{MK}^J$ extracts the component of angular momentum along the intrinsic axis z defined by K. The Wigner D-function is defined as $D_{MK}^J(\Omega) \equiv \langle JM| \hat{R}(\Omega) |JK\rangle = \langle JM| e^{i\phi\hat{J}_z} e^{i\theta\hat{J}_y} e^{i\psi\hat{J}_z} |JK\rangle$, where $\Omega = (\phi, \theta, \psi)$ represents the three Euler angles. The $\hat{N} = \sum_k a_k^\dagger a_k$ is particle-number operator. The mean-field configurations $|\Phi_\kappa^{(\mathrm{OA})}(\mathbf{q})\rangle$ for odd-mass nuclei can be constructed as one-quasiparticle excitations on even-even vacua [2],

$$|\Phi_\kappa^{(\mathrm{OA})}(\mathbf{q})\rangle = \alpha_\kappa^\dagger |\Phi_{(\kappa)}(\mathbf{q})\rangle, \quad \alpha_\kappa |\Phi_{(\kappa)}(\mathbf{q})\rangle = 0, \tag{18}$$

where $|\Phi_{(\kappa)}(\mathbf{q})\rangle$ is a HFB state with even-number parity labeled with the collective coordinate $\mathbf{q}$. The quasiparticle operators $(\alpha, \alpha^\dagger)$ are connected to single-particle operators $(a, a^\dagger)$ via the Bogoliubov transformation [2],

$$\begin{pmatrix} \alpha \\ \alpha^\dagger \end{pmatrix} = \begin{pmatrix} U^\dagger & V^\dagger \\ V^T & U^T \end{pmatrix} \begin{pmatrix} a \\ a^\dagger \end{pmatrix}, \tag{19}$$

where the U, V matrices are determined by the minimization of particle-number projected energy,

$$\delta \frac{\langle \Phi_\kappa^{(\mathrm{OA})}(\mathbf{q})| \hat{\mathcal{H}} \hat{P}^N \hat{P}^Z |\Phi_\kappa^{(\mathrm{OA})}(\mathbf{q})\rangle}{\langle \Phi_\kappa^{(\mathrm{OA})}(\mathbf{q})| \hat{P}^N \hat{P}^Z |\Phi_\kappa^{(\mathrm{OA})}(\mathbf{q})\rangle} = 0. \tag{20}$$

Different from the recent study based on a covariant EDF in Ref. [26], where three different schemes were employed to construct the configurations for odd-mass nuclei within the BCS ansatz, in this work we obtain the configurations of one-quasiparticle states with odd-number parity self-consistently by simply exchanging the k-column of the U and V matrices in the HFB wave function [2]:

$$(U_{pk}, V_{pk}) \longleftrightarrow (V_{pk}^*, U_{pk}^*), \tag{21}$$

where the index $p = (\tau n \ell j m)_p \equiv (n_p, \xi_p)$ is a label for the spherical harmonic oscillator basis, and k the label for a quasiparticle state. For simplicity, axial symmetry is assumed. In this case, quasiparticle states are labeled with quantum numbers K^π, where $K = |m_p|$ with m_p being the projection of angular momentum j_p along z-axis, and parity $\pi = (-1)^{\ell_p}$. The collective coordinate $\mathbf{q}$ is replaced with the dimensionless quadrupole deformation β_2,

$$\beta_2 = \frac{4\pi}{3AR^2} \langle \Phi_\kappa^{(\mathrm{OA})}(\mathbf{q})| r^2 Y_{20} |\Phi_\kappa^{(\mathrm{OA})}(\mathbf{q})\rangle . \tag{22}$$

The U and V matrices are determined from the HFB calculation within the scheme of variation after particle-number projection (VAPNP), in which a gradient descent method is exploited to minimize the expectation value of the Hamiltonian with respect to the particle-number projected HFB state. For details, see, for instance, Refs. [2,31,32]. We note that the Kramers' degeneracy is lifted due to the breaking of time-reversal invariance in the self-consistent HFB calculation.

The weight function $f_c^{J\alpha\pi}$ of the state (15) is determined by the variational principle, which leads to the following Hill–Wheeler–Griffin (HWG) Equation [2,7]:

$$\sum_{c'} \left[\mathscr{H}_{cc'}^{NZJ\pi} - E_\alpha^J \mathscr{N}_{cc'}^{NZJ\pi} \right] f_{c'}^{J\alpha\pi} = 0, \tag{23}$$

where the Hamiltonian kernel and norm kernel are defined by

$$\begin{aligned} \mathscr{O}_{cc'}^{NZJ\pi} &= \langle NZJ\pi; c| \hat{O} |NZJ\pi; c'\rangle \\ &= \frac{2J+1}{8\pi^2} \int d\Omega D_{KK'}^{J*}(\Omega) \int_0^{2\pi} d\varphi_n \frac{e^{-iN\varphi_n}}{2\pi} \int_0^{2\pi} d\varphi_p \frac{e^{-iZ\varphi_p}}{2\pi} \\ &\quad \times \langle \Phi_\kappa^{(\mathrm{OA})}(\mathbf{q})| \hat{O} \hat{R}(\Omega) e^{i\hat{Z}\varphi_p} e^{i\hat{N}\varphi_n} |\Phi_{\kappa'}^{(\mathrm{OA})}(\mathbf{q}')\rangle , \end{aligned} \tag{24}$$

with the operator $\hat{O}$ representing $\hat{\mathcal{H}}$ and 1, respectively. The parity π is defined by the quasiparticle configurations $|\Phi_\kappa^{(\mathrm{OA})}(\mathbf{q})\rangle$.

The HWG Equation (23) for a given set of quantum numbers (NZJ) is solved in the standard way as discussed in Refs. [2,33]. It is accomplished by diagonalizing the norm kernel $\mathscr{N}_{cc'}^{NZJ\pi}$ first. A new set of basis is constructed using the eigenfunctions of the norm kernel with eigenvalue larger than a pre-chosen cutoff value to remove possible redundancy in the original basis. The Hamiltonian is diagonalized in this new basis. In this way, one is able to obtain the energies E_α^J and the mixing weights $f_c^{J\alpha\pi}$ of nuclear states $|\Psi_\alpha^{J\pi}\rangle$. Since the basis functions $|NZJ; c\rangle$ are nonorthogonal to each other, one usually introduces the collective wave function $g_\alpha^{J\pi}(K, \mathbf{q})$ as below

$$g_\alpha^{J\pi}(K, \mathbf{q}) = \sum_{c'} (\mathscr{N}^{1/2})_{c,c'}^{NZJ\pi} f_{c'}^{J\alpha\pi}, \tag{25}$$

which fulfills the normalization condition. The distribution of $g_\alpha^{J\pi}(K,\mathbf{q})$ over K and $\mathbf{q}$ reflects the contribution of each basis function to the nuclear state $|\Psi_\alpha^{J\pi}\rangle$.

2.3. Evaluation of Norm and Hamiltonian Overlaps

The energy overlap is defined as the ratio of Hamiltonian overlap to the norm overlap,

$$\begin{aligned} E(\kappa\mathbf{q},\kappa'\mathbf{q}';g) &\equiv \frac{\langle\Phi_\kappa^{(\mathrm{OA})}(\mathbf{q})|\,\hat{\mathcal{H}}\hat{R}(\Omega)e^{i\hat{Z}\varphi_p}e^{i\hat{N}\varphi_n}\,|\Phi_{\kappa'}^{(\mathrm{OA})}(\mathbf{q}')\rangle}{\langle\Phi_\kappa^{(\mathrm{OA})}(\mathbf{q})|\,\hat{R}(\Omega)e^{i\hat{Z}\varphi_p}e^{i\hat{N}\varphi_n}\,|\Phi_{\kappa'}^{(\mathrm{OA})}(\mathbf{q}')\rangle} \\ &= \mathscr{E}+\sum_{pq}\mathscr{F}_q^p\tilde{\rho}_q^p(\kappa\mathbf{q},\kappa'\mathbf{q}';g)+\frac{1}{4}\sum_{pqrs}\mathscr{V}_{rs}^{pq}\tilde{\rho}_{rs}^{pq}(\kappa\mathbf{q},\kappa'\mathbf{q}';g), \end{aligned} \tag{26}$$

where g stands for the set of parameters $\{\Omega,\varphi_n,\varphi_p\}$. The matrix elements of the mixed one-body densities and pairing tensors, hatted with the symbol $\sim$, are defined as

$$\tilde{\rho}_q^p(\kappa\mathbf{q},\kappa'\mathbf{q}';g) \equiv \frac{\langle\Phi_\kappa^{(\mathrm{OA})}(\mathbf{q})|\,a_p^\dagger a_q\hat{R}(\Omega)e^{i\hat{Z}\varphi_p}e^{i\hat{N}\varphi_n}\,|\Phi_{\kappa'}^{(\mathrm{OA})}(\mathbf{q}')\rangle}{\langle\Phi_\kappa^{(\mathrm{OA})}(\mathbf{q})|\,\hat{R}(\Omega)e^{i\hat{Z}\varphi_p}e^{i\hat{N}\varphi_n}\,|\Phi_{\kappa'}^{(\mathrm{OA})}(\mathbf{q}')\rangle}, \tag{27}$$

$$\tilde{\kappa}^{pq}(\kappa\mathbf{q},\kappa'\mathbf{q}';g) \equiv \frac{\langle\Phi_\kappa^{(\mathrm{OA})}(\mathbf{q})|\,a_p^\dagger a_q^\dagger\hat{R}(\Omega)e^{i\hat{Z}\varphi_p}e^{i\hat{N}\varphi_n}\,|\Phi_{\kappa'}^{(\mathrm{OA})}(\mathbf{q}')\rangle}{\langle\Phi_\kappa^{(\mathrm{OA})}(\mathbf{q})|\,\hat{R}(\Omega)e^{i\hat{Z}\varphi_p}e^{i\hat{N}\varphi_n}\,|\Phi_{\kappa'}^{(\mathrm{OA})}(\mathbf{q}')\rangle}, \tag{28}$$

$$\tilde{\kappa}_{rs}(\kappa\mathbf{q},\kappa'\mathbf{q}';g) \equiv \frac{\langle\Phi_\kappa^{(\mathrm{OA})}(\mathbf{q})|\,a_s a_r\hat{R}(\Omega)e^{i\hat{Z}\varphi_p}e^{i\hat{N}\varphi_n}\,|\Phi_{\kappa'}^{(\mathrm{OA})}(\mathbf{q}')\rangle}{\langle\Phi_\kappa^{(\mathrm{OA})}(\mathbf{q})|\,\hat{R}(\Omega)e^{i\hat{Z}\varphi_p}e^{i\hat{N}\varphi_n}\,|\Phi_{\kappa'}^{(\mathrm{OA})}(\mathbf{q}')\rangle}. \tag{29}$$

The matrix elements of the mixed two-body density are determined by the generalized Wick theorem [34],

$$\begin{aligned} \tilde{\rho}_{rs}^{pq}(\kappa\mathbf{q},\kappa'\mathbf{q}';g) &\equiv \frac{\langle\Phi_\kappa^{(\mathrm{OA})}(\mathbf{q})|\,a_p^\dagger a_q^\dagger a_s a_r\hat{R}(\Omega)e^{i\hat{Z}\varphi_p}e^{i\hat{N}\varphi_n}\,|\Phi_{\kappa'}^{(\mathrm{OA})}(\mathbf{q}')\rangle}{\langle\Phi_\kappa^{(\mathrm{OA})}(\mathbf{q})|\,\hat{R}(\Omega)e^{i\hat{Z}\varphi_p}e^{i\hat{N}\varphi_n}\,|\Phi_{\kappa'}^{(\mathrm{OA})}(\mathbf{q}')\rangle} \\ &= \tilde{\rho}_r^p\tilde{\rho}_s^q-\tilde{\rho}_s^p\tilde{\rho}_r^q+\tilde{\kappa}^{pq}\tilde{\kappa}_{rs}. \end{aligned} \tag{30}$$

With the above relation, the energy overlap can be rewritten as below,

$$E(\kappa\mathbf{q},\kappa'\mathbf{q}';g) = \mathscr{E}+\sum_{pq}\mathscr{F}_q^p\tilde{\rho}_q^p+\frac{1}{2}\sum_{pq}\left(\tilde{\Gamma}_q^p\tilde{\rho}_q^p+\tilde{\Delta}^{pq}\tilde{\kappa}_{pq}\right), \tag{31}$$

where the matrix elements of the mixed particle-hole field $\tilde{\Gamma}$ and particle-particle field $\tilde{\Delta}$ are defined as

$$\tilde{\Gamma}_q^p\equiv\sum_{pqrs}\mathscr{V}_{qs}^{pr}\tilde{\rho}_s^r,\quad \tilde{\Delta}^{pq}\equiv\frac{1}{2}\sum_{rs}\mathscr{V}_{pq}^{rs}\tilde{\kappa}^{rs}. \tag{32}$$

It is efficient to compute the energy overlap directly in the J-coupled scheme.

- The contribution of the one-body term is simply given by

$$E^{(1B)}=\sum_{pq}\delta_{j_pj_q}\hat{j}_p\mathscr{F}_{(qp)}^0\tilde{\rho}_{(qp)00}, \tag{33}$$

where $\hat{j}_p\equiv\sqrt{2j_p+1}$. The reduced matrix element is defined as $\mathscr{F}_{qp}^0=\langle q||\mathscr{F}_0||p\rangle$, and the one-body density operator with the two angular momenta coupled to zero [13]

$$\hat{\rho}_{(qp)00}\equiv\frac{\left[a_q^\dagger\tilde{a}_p\right]_{00}}{\sqrt{2j_q+1}}\delta_{\xi_q\xi_p} \tag{34}$$

with $\tilde{a}_{nljm} \equiv (-1)^{j+m} a_{nlj-m}$.

- The energy by the two-body term consists of pp term

$$E_{pp}^{(2B)} = -\frac{1}{4} \sum_{abcd,L} \mathcal{V}^{L}_{(ab)(cd)} \sum_{M_L} (-1)^{L-M_L} \tilde{\kappa}^{(01)}_{(ab)LM_L} \tilde{\kappa}^{(10)}_{(cd)L-M_L} \tag{35}$$

and ph term

$$E_{ph}^{(2B)} = \frac{1}{2} \sum_{abcd,L} \mathcal{V}^{L}_{(a\bar{b})(c\bar{d})} \sum_{M_L} \tilde{\rho}_{(ba)LM_L} \tilde{\rho}^{\dagger}_{(dc)L-M_L} \tag{36}$$

where the J-coupled mixed density and pairing density are defined as,

$$\tilde{\rho}_{(ba)LM_L} = \sum_{m_a m_b} s_b \langle j_a m_a j_b - m_b | LM_L \rangle \tilde{\rho}^{a}_{b}, \tag{37a}$$

$$\tilde{\rho}^{\dagger}_{(dc)L-M_L} = \sum_{m_c m_d} s_d \langle j_c m_c j_d - m_d | L - M_L \rangle (\tilde{\rho}^{c}_{d})^{\dagger}, \tag{37b}$$

$$\tilde{\kappa}^{(01)}_{(ab)LM_L} = \sum_{m_a m_b} \langle j_a m_a j_b m_b | LM_L \rangle \tilde{\kappa}^{ab}, \tag{37c}$$

$$\tilde{\kappa}^{(10)}_{(cd)L-M_L} = (-1)^{L+M_L} \sum_{m_c m_d} \langle j_c m_c j_d m_d | LM_L \rangle (\tilde{\kappa}_{cd})^{\dagger}. \tag{37d}$$

Here, we introduce the symbol $s_b \equiv (-1)^{j_b - m_b}$. The symmetry of Clebsch–Gordan coefficient $\langle j_a m_a j_b - m_b | LM_L \rangle$ implies the relation $\tilde{\rho}_{(ba)LM_L} = (-1)^{L-(j_a+j_b)+1} \tilde{\rho}_{(ab)LM_L}$. The ph-type two-body interaction matrix elements in the J-coupled form are related to those of pp-type via the Pandya transformation [35],

$$\mathcal{V}^{J}_{(i\bar{j})(k\bar{l})} = -\sum_{L} \hat{L}^2 \begin{Bmatrix} j_i & j_j & J \\ j_k & j_l & L \end{Bmatrix} \mathcal{V}^{L}_{(i\bar{l})(kj)}, \tag{38}$$

where the unnormalized pp-type two-body matrix elements in the J-coupled form are related to those in M-scheme as follows:

$$\mathcal{V}^{J}_{(ij)(kl)} = \sum_{m_i m_j m_k m_l} \langle j_i m_i j_j m_j | JM \rangle \langle j_k m_k j_l m_l | JM \rangle \mathcal{V}^{ij}_{kl}. \tag{39}$$

The norm overlap of the HFB wave functions with odd-number parity is computed with the Pfaffian formula in Refs. [36,37].

3. Results and Discussion

Effective Hamiltonians

In this work, the NN interaction $V^{(2)}_{ij}$ in Equation (1) is chosen as the chiral N^{3}LO interaction by Entem and Machleidt [38], denoted as "EM". We utilize the free-space SRG [39] to evolve the EM interaction to a resolution scale of $\lambda = 1.8$ fm^{-1}. The $3N$ interaction $W^{(3)}_{ijk}$ is directly constructed with a cutoff of $\Lambda = 2.0$ fm^{-1}. The Hamiltonian is referred to as EMλ/Λ, i.e., EM1.8/2.0, which was fitted to NN scattering phase shifts, the binding energy of ^{3}H, and the charge radius of ^{4}He, see Ref. [40] for details. For the $3N$ interaction, we discard all matrix elements involving states with $e_1 + e_2 + e_3 > 14$, where $e_i = 2n_i + \ell_i$ denotes the number of oscillator quanta in state i. The maximal value of e_i is labeled with $e_{\max}$, and the frequency of the harmonic oscillator basis is chosen as $\hbar\omega = 20$ MeV. Starting from the chiral $NN + 3N$ interaction, we produce three sets of effective Hamiltonians labeled as `magic-Ne20`, `magic-Ne22`, and `magic-ENO/EW`, respectively. These Hamiltonians are generated by normal-ordering the $3N$ interaction with respect to the reference states of spherical particle-number projected HFB states for ^{20}Ne, ^{22}Ne, and their ensemble with equal weights. The residual normal-ordered three-body

term, c.f. Figure 1d, is neglected. Table 1 lists the expectation value of each term in the three types of effective Hamiltonians $\mathcal{H}_0$ in (11) with respect to the corresponding reference state. One can see that in the case without the 3N interaction, the unnormal-ordering form of the Hamiltonian $\mathcal{H}_0$ returns back to the original Hamiltonian $\hat{H}_0$.

For the case with $e_{\max} = 6$, the relative contribution of each term in different effective Hamiltonians to the energy is compared in Table 1. The contribution of the 3N interaction to energy, c.f. Figure 1a, is given by

$$E_0^{(3)} = \frac{1}{36} \sum_{pqrstu} w_{rsu}^{pqt} \left(6\lambda_s^p \lambda_t^q \lambda_u^r + 9\lambda_s^p \lambda_{tu}^{qr} + \lambda_{rsu}^{pqt} \right). \tag{40}$$

Comparing the E_0 value in the third row of Table 1, labeled by `Ne20` with the E_0 value in the last row, labeled by `Ne20 (w/o 3N)`, one finds the contribution of the 3N interaction to the energy $E_0^{(3)} = 80.338$ MeV. On the other hand, the zero-point energy $\mathscr{E}_0$ in (12) of the unnormal-ordered Hamiltonian in the first row

$$\mathscr{E}_0 = \frac{1}{36} \sum_{pqrstu} w_{stu}^{pqr} \left(6\lambda_s^p \lambda_t^q \lambda_u^r - 9\lambda_{st}^{pq} \lambda_u^r + \lambda_{stu}^{pqr} \right) \tag{41}$$

is 50.093 MeV. Their difference gives

$$\frac{1}{2} \sum_{pqrstu} w_{stu}^{pqr} \lambda_{st}^{pq} \lambda_u^r = 30.245 \quad \text{MeV}. \tag{42}$$

Since the term depending on λ_{stu}^{pqr} is much smaller than the other terms, we drop this term out and find the term,

$$\frac{1}{6} \sum_{pqrstu} w_{rsu}^{pqt} \lambda_s^p \lambda_t^q \lambda_u^r = 65.215 \quad \text{MeV} \tag{43}$$

depending solely on the one-body density, provides the predominant contribution to energies $E_0^{(3)}$ and $\mathscr{E}_0$. Subsequently, we carry out PGCM calculations for low-lying states of ^{21}Ne using the above effective Hamiltonians.

Table 1. The expectation value (in MeV) of each term in the effective Hamiltonians $\mathcal{H}_0$ in (11), derived from the nuclear chiral interaction EM1.8/2.0 on the basis of the spherical particle-number projected HFB state for ^{20}Ne, ^{22}Ne, and their ensemble with equal weights (ENO/EW), respectively, where $e_{\max} = 6$, and $\hbar\omega = 20$ MeV.

Interactions	$e_{\max}$	E_0	$\langle \mathcal{F} \rangle$	$\langle \mathcal{V} \rangle$	$\mathscr{E}_0$
`Ne20`	6	−96.931	211.205	−358.229	50.093
`ENO/EW`	6	−101.781	225.067	−381.555	54.706
`Ne22`	6	−109.034	242.241	−408.614	57.339
`Ne20(w/o 3N)`	6	−177.269	506.122	−683.391	0

Figures 2 and 3 show the change in the effective single-particle energies (ESPEs) with the quadrupole deformation β_2 from the PNP+HFB (VAPNP) calculation for the HFB states, where the ESPE ε_k is obtained from the diagonalization of the single-particle Hamiltonian,

$$\begin{aligned} h_q^p &= \mathscr{F}_q^p + \sum_{rs} \mathscr{V}_{qs}^{pr} \rho_s^r \\ &= \bar{t}_q^p + \sum_{rs} \bar{v}_{qs}^{pr} \rho_s^r + \frac{1}{4} \sum_{rstu} w_{qsu}^{prt} \gamma_{su}^{rt} + \sum_{rstu} w_{qsu}^{prt} \gamma_s^r (\rho_u^t - \gamma_u^t), \end{aligned} \tag{44}$$

where γ^t_u is the one-body density of the correlated state, and ρ^r_s is the one-body density of mean-field state $|\Phi^{(\mathrm{OA})}_\kappa(\mathbf{q})\rangle$ defined by

$$\rho^r_s \equiv \langle \Phi^{(\mathrm{OA})}_\kappa(\mathbf{q})|\, a^\dagger_r a_s \,|\Phi^{(\mathrm{OA})}_\kappa(\mathbf{q})\rangle\,. \tag{45}$$

It is shown in Figure 2 that the neutron partner states with the same value of $|m|$, related by the time-reversal operator, are not degenerate in the HFB states for ^{21}Ne with odd-number parity. A comparison is made between the ESPEs obtained by the effective Hamiltonians `magic-Ne20` and `magic-Ne22`. The lifting of Kramers' degeneracy in the HFB states for ^{21}Ne results in non-degeneracy among time-reversal states with identical values of $|m|$. For clarity, only the energy of one of the time-reversal states is depicted in Figure 3. It is observed that the ESPEs from the two effective Hamiltonians are difficult to distinguish.

Before presenting the projected energy curves with different angular momenta, we examine the issues of singularity and finite steps found in the MR-EDF [27–29]. Figure 4 displays the energies (normalized to the converged values) of particle-number projected HFB states for ^{21}Ne with $K^\pi = 1/2^+$ and quadrupole deformation $\beta_2 = 0.0$, as a function of the number N_φ of meshpoints in the gauge angle φ. The Fomenko expansion method [41] is used for the particle-number projection, where the k-th gauge angle φ_k is chosen as $2\pi(k/N_\varphi)$. It is observed that the energy remains constant for $N_\varphi \geq 5$, regardless of whether N_φ is an even or odd number. For comparison, we also show the results from the calculations by artificially multiplying a factor of 1.1 to the two-body interaction matrix elements for the mixed particle-hole field. In this case, dips are indeed observed at $N_\varphi = 20, 40, 60, \ldots$, corresponding to the situation where the gauge angle $\varphi_k = \pi/2$ is chosen at the meshpoints with $k = 5, 10, 15, \ldots$, respectively. It demonstrates numerically that one should use the same interaction matrix elements for both the particle-hole and particle-particle channels, in which case one will be free of the problem of singularity.

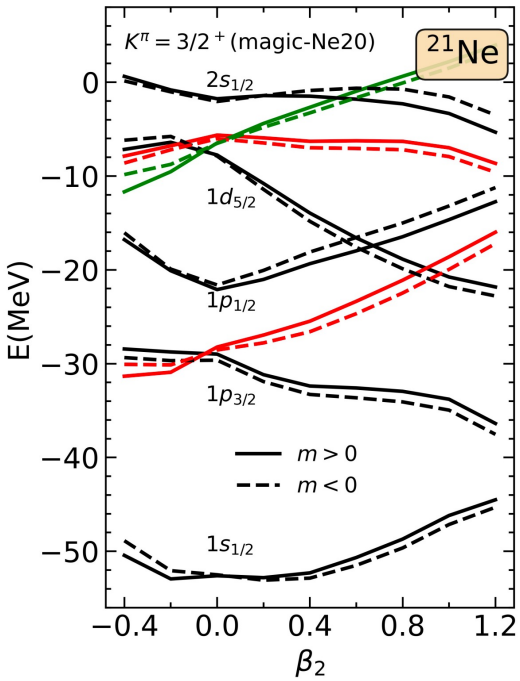

Figure 2. The effective single-particle energies of neutron states with $m > 0$ (solid lines) and $m < 0$ (dashed lines) as a function of quadrupole deformation β_2 from the PNP + HFB (VAPNP) calculation for the HFB states with $K^\pi = 3/2^+$ using the effective Hamiltonians `magic-Ne20`. The states with $|m| = 1/2$, $|m = 3/2|$ and $|m = 5/2|$ are plotted in black, red and green colors, respectively.

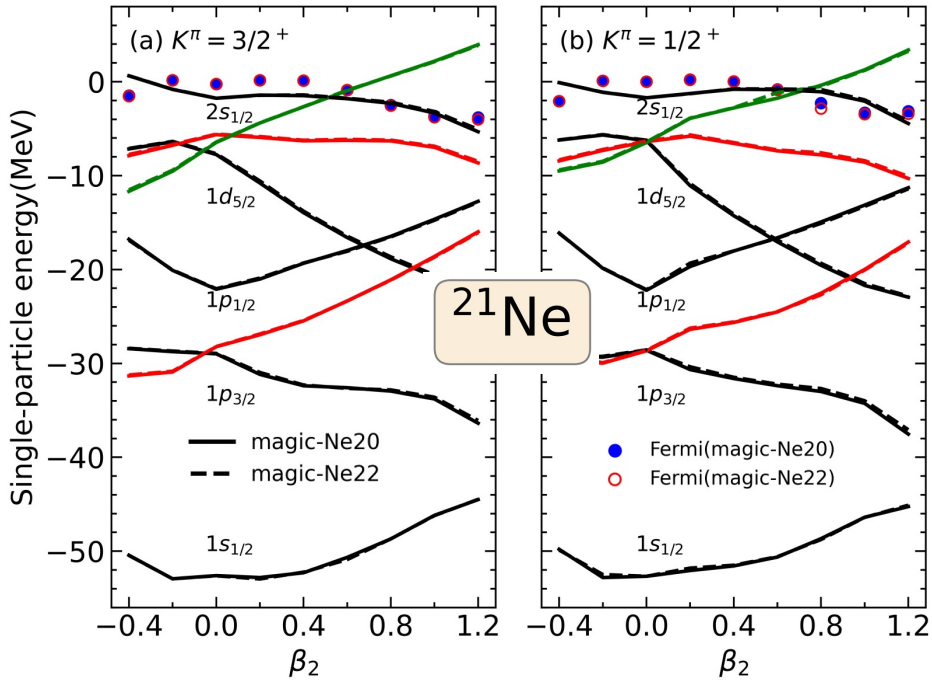

Figure 3. The effective single-particle energies of neutron states (with $m > 0$) from the PNP+HFB (VAPNP) calculation for the HFB states with $K^\pi = 3/2^+$ (**a**) and $K^\pi = 1/2^+$ (**b**), where the effective Hamiltonians `magic-Ne20` (solid) and `magic-Ne22` (dashed lines) are employed, respectively. The Fermi energies are indicated with dots. The states with $|m| = 1/2$, $|m = 3/2|$ and $|m = 5/2|$ are plotted in black, red and green colors, respectively.

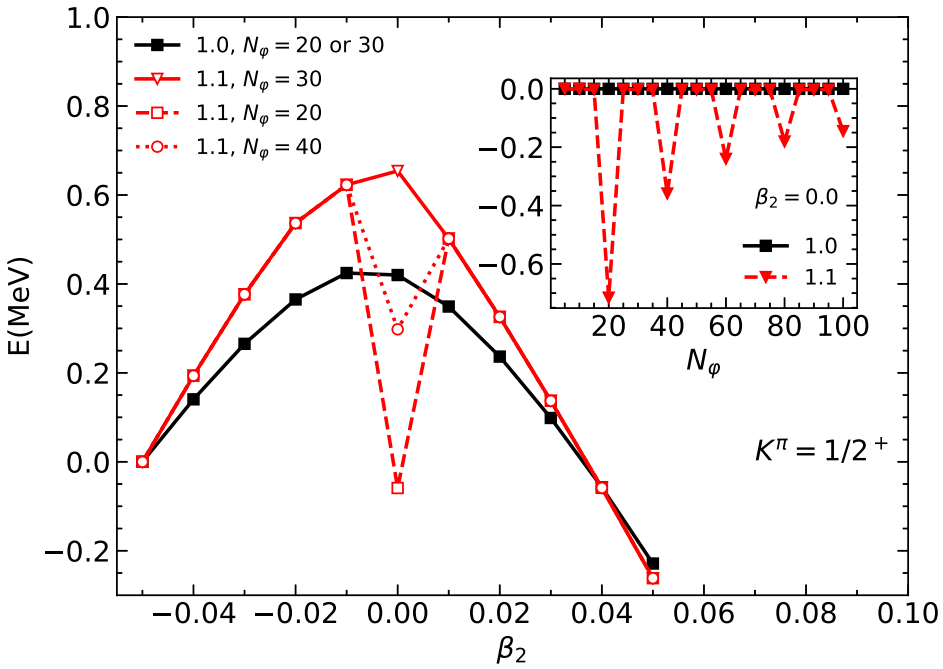

Figure 4. The energies of particle-number projected HFB states for ^{21}Ne with $K^\pi = 1/2^+$ as a function of quadrupole deformation β_2, where the number N_φ of meshpoints in the gauge angle φ is chosen as 20, 30, and 40, respectively. The results from the calculations by multiplying a factor of 1.1 artificially to the two-body interaction matrix elements for the mixed field $\tilde{\Gamma}$ are given for comparison. The inset shows the energy of spherical state normalized to the converged value as a function of N_φ.

Figure 5 displays the energy curves of particle-number projected HFB states for ^{21}Ne with $K^\pi = 3/2^+$ and $1/2^+$, respectively. The HFB wave functions are obtained from the PNP-HFB (VAPNP) calculations using the Hamiltonian $\hat{\mathcal{H}}_0$, with the $3N$ interaction normal-ordered with respect to the references of ^{20}Ne, ^{22}Ne, and their ensemble with equal weights, respectively. It can be observed that the global energy minima of all three curves are located in prolate states with quadrupole deformation β_2 between 0.4 and 0.5. The configurations with $K^\pi = 3/2^+$ are globally lower than those with $K^\pi = 1/2^+$. Furthermore, the configurations based on different Hamiltonians are systematically shifted from each other in energy by less than one MeV.

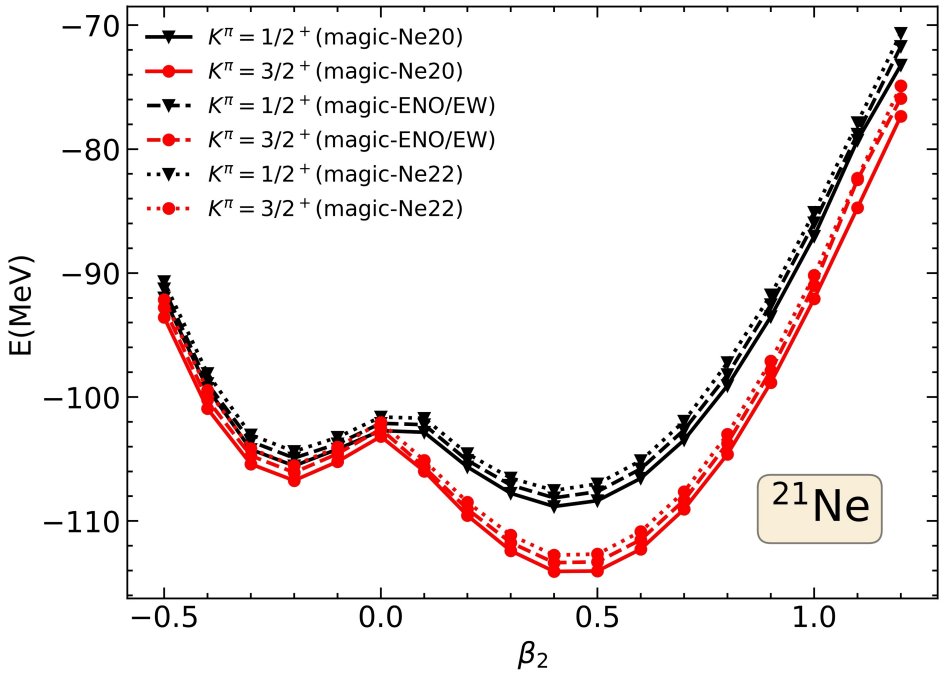

Figure 5. The energies of mean-field states $|\Phi_\kappa^{(\mathrm{OA})}(\mathbf{q})\rangle$ for ^{21}Ne with $K^\pi = 1/2^+, 3/2^+$ as a function of intrinsic quadrupole deformation β_2 from the PNP-HFB (VAPNP) calculation, where the three types of Hamiltonians $\hat{\mathcal{H}}_0$, i.e., `magic-Ne20, magic-Ne22, and magic-ENO/EW`, are employed. The harmonic oscillator basis is chosen as $e_{\max} = 6$, $\hbar\omega = 20$ MeV. See the main text for details.

Figure 6 displays the energies of states with projection onto the correct particle numbers and $J^\pi = 3/2^+, 5/2^+$, and $7/2^+$ for ^{21}Ne with $K^\pi = 3/2^+$ and $K^\pi = 1/2^+$, respectively. The effective Hamiltonians used are `HO` with and without the $3N$ interaction. It is shown that the quadrupole deformation parameter β_2 of the prolate energy-minimal state by the `HO (w/o 3N)` is smaller than the other two cases. Additionally, the energy curve with the increase in β_2 is also stiffer than that with the $3N$ interaction.

Figure 7 shows a comparison of the energy spectra for ^{21}Ne from configuration-mixing calculations with different Hamiltonians. The states with the same K^π are grouped into the same column. The main features of the two bands with $K^\pi = 3/2^+$ and $1/2^+$ are reproduced, although the excitation energies of the states belonging to the $1/2^+$ band are systematically overestimated. The mixing of quasiparticle excitation configurations is expected to lower the entire $K^\pi = 1/2^+$ band. In Figure 7c, one can observe that the energy spectra from the `magic-Ne20` and `magic-Ne22` Hamiltonians are very close to each other. The high-lying states from `magic-Ne22` are slightly lower than those from `magic-Ne20`. In Figure 7b, the energy spectra become more stretched when the $3N$ interaction is turned off. We note that the ground-state energy from the pure PGCM calculation with the chiral $NN + 3N$ interaction is systematically underestimated. According to Ref. [14], one may gain more correlation energy by implementing the multi-reference in-medium similarity renormalization group (MR-IMSRG) [42] and increasing the value of $e_{\max}$.

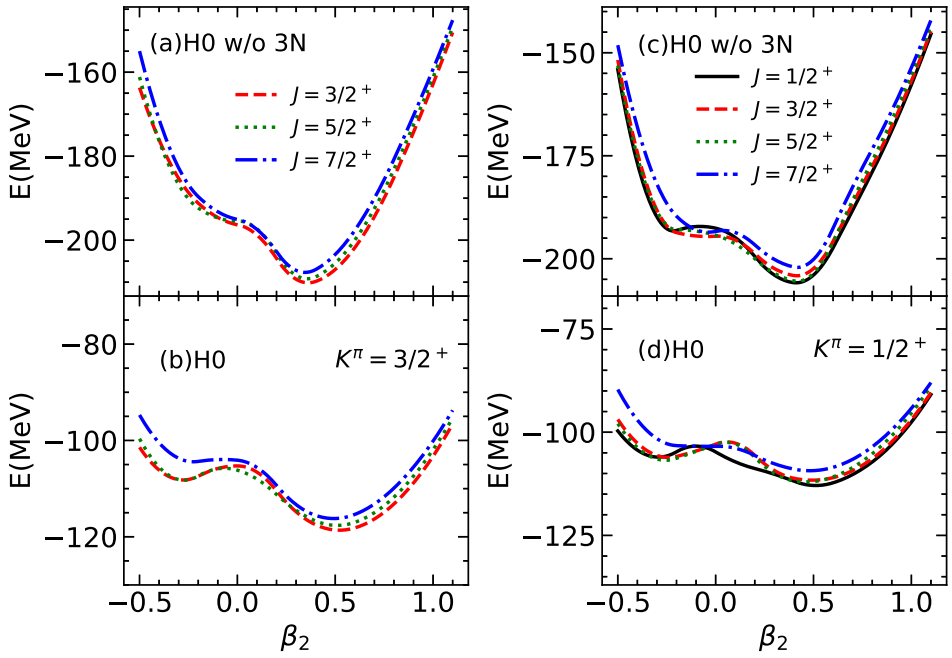

Figure 6. The energies of states with projection onto particle numbers ($N = 11, Z = 10$) and spin-parity $J^\pi = 3/2^+, 5/2^+$ and $7/2^+$ for ^{21}Ne with quantum numbers $K^\pi = 3/2^+$ (**left panels**) and $K^\pi = 1/2^+$ (**right panels**) as a function of the quadrupole deformation parameter β_2. The results of calculations without the $3N$ interaction are given in (**a**,**c**), and those with the $3N$ interaction are given in (**b**,**d**). See the main text for details.

The collective wave functions of the low-lying states with different J^π, and $K^\pi = 3/2^+$ and $1/2^+$, by the `magic-Ne20` effective Hamiltonian, are displayed in Figure 8. It is shown that in all cases, the wave functions are peaked around $\beta_2 = 0.4$ and do not change significantly with the increase in angular momentum, implying the stability of the shapes in the low-lying states.

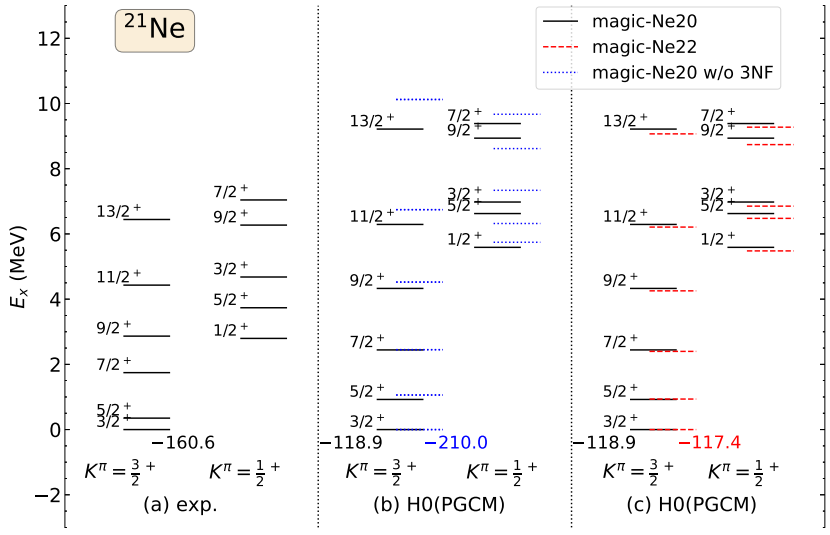

Figure 7. The energy spectra of low-lying states in ^{21}Ne with $K^\pi = 3/2^+$ and $1/2^+$. Experimental data from Ref. [43] are shown in (**a**). The results by the Hamiltonians `H0` with and without the $3N$ interaction based on the reference state of ^{20}Ne are displayed in (**b**). The results by the Hamiltonians `H0` based on the reference state of ^{20}Ne and ^{22}Ne are compared in (**c**). The total energy of ground state in each case is also provided. See the main text for details.

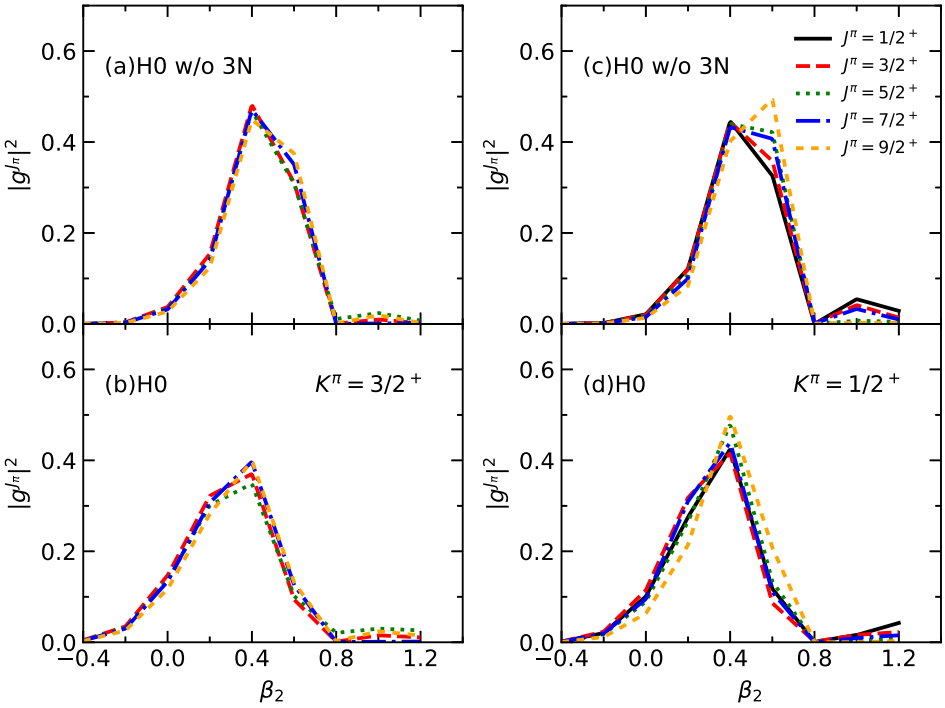

Figure 8. The distribution of collective wave functions $|g_\alpha^{J\pi}|^2$, defined in (25), as a function of quadrupole deformation β_2 for the low-lying states of ^{21}Ne with $K^\pi = 3/2^+$ (**left panels**) and $K^\pi = 1/2^+$ (**right panels**), respectively. The energy of the ground-state in each case is also provided. The results of calculations without the $3N$ interaction are given in (**a**,**c**), and those with the $3N$ interaction are given in (**b**,**d**). See the main text for details.

4. Conclusions

We have extended PGCM for the low-lying states of ^{21}Ne, starting from a chiral two-plus-three-nucleon interaction, and compared the results obtained using effective Hamiltonians derived with the three-nucleon interaction normal-ordered with the following three different reference states: particle-number projected HFB states for ^{20}Ne, ^{22}Ne, and an ensemble with equal weights. The topology of the potential energy surfaces shows no significant differences among the three effective Hamiltonians, even though they exhibit a systematic energy shift of less than one MeV. The excitation energies of the low-lying states of ^{21}Ne by the effective Hamiltonian based on the reference state of ^{20}Ne are slightly larger than those by the effective Hamiltonian of ^{22}Ne. Furthermore, we demonstrate that the three-nucleon interaction notably affects the low-lying states, i.e., the energy spectrum becomes stretched and the quadrupole collectivity is reduced.

Next, we will extend the in-medium GCM [13,14], namely, the combination of PGCM with the ab initio method of MR-IMSRG, to study the low-lying states of odd-mass nuclei using the consistently evolved operators. The results of this study will be published elsewhere, separately.

Author Contributions: Conceptualization and methodology, W.L., J.Y. and H.H.; validation, W.L. and E.Z.; writing—original draft preparation, W.L. and J.Y.; writing—review and editing, H.H., W.L., J.Y. and E.Z. All authors have read and agreed to the published version of the manuscript.

Funding: This research was funded in part by the National Natural Science Foundation of China (Grant Nos. 12375119, 12141501), Guangdong Basic and Applied Basic Research Foundation (2023A1515010936) and the Fundamental Research Funds for the Central Universities, Sun Yat-sen University. H.H. was funded by the U.S. Department of Energy, Office of Science, Office of Nuclear Physics DE-SC0023516 and DE-SC0023175 (SciDAC-5 NUCLEI Collaboration).

Data Availability Statement: The data presented in this study are available on request from the corresponding author.

Acknowledgments: We thank K. Hebeler for providing the three-nucleon interaction in momentum space.

Conflicts of Interest: The authors declare no conflicts of interest.

Abbreviations

The following abbreviations are used in this manuscript:

EFT	Effective field theory
IMSRG	In-medium similarity renormalization group
PGCM	Projected generator coordinate method
IM-GCM	In-medium generator coordinate method
MR-CDFT	Multi-reference covariant density functional theory
HWG	Hill–Wheeler–Griffin

References

1. Bohr, A.; Mottelson, B.R. *Nuclear Structure. Volume II. Nuclear Deformations*; Word Scientific: Singapore, 1998.
2. Ring, P.; Schuck, P. *The Nuclear Many-Body Problem*; Springer: New York, NY, USA, 1980.
3. Engel, J.; Ramsey-Musolf, M.J.; van Kolck, U. Electric Dipole Moments of Nucleons, Nuclei, and Atoms: The Standard Model and Beyond. *Prog. Part. Nucl. Phys.* **2013**, *71*, 21–74. [CrossRef]
4. Arrowsmith-Kron, G.; Athanasakis-Kaklamanakis, M.; Au, M.; Ballof, J.; Berger, R.; Borschevsky, A.; Breier, A.A.; Buchinger, F.; Budker, D.; Caldwell, L.; et al. Opportunities for Fundamental Physics Research with Radioactive Molecules. *arXiv* **2023**, arXiv:2302.02165.
5. Brodeur, M.; Buzinsky, N.; Caprio, M.A.; Cirigliano, V.; Clark, J.A.; Fasano, P.J.; Formaggio, J.A.; Gallant, A.T.; Garcia, A.; Gandolfi, S.; et al. Nuclear β decay as a probe for physics beyond the Standard Model. *arXiv* **2023**, arXiv:2301.03975.
6. Yao, J.M.; Meng, J.; Niu, Y.F.; Ring, P. Beyond-mean-field approaches for nuclear neutrinoless double beta decay in the standard mechanism. *Prog. Part. Nucl. Phys.* **2022**, *126*, 103965. [CrossRef]
7. Hill, D.L.; Wheeler, J.A. Nuclear constitution and the interpretation of fission phenomena. *Phys. Rev.* **1953**, *89*, 1102–1145. [CrossRef]
8. Griffin, J.J.; Wheeler, J.A. Collective Motions in Nuclei by the Method of Generator Coordinates. *Phys. Rev.* **1957**, *108*, 311–327. [CrossRef]
9. Bender, M.; Heenen, P.H.; Reinhard, P.G. Self-consistent mean-field models for nuclear structure. *Rev. Mod. Phys.* **2003**, *75*, 121–180. [CrossRef]
10. Niksic, T.; Vretenar, D.; Ring, P. Relativistic Nuclear Energy Density Functionals: Mean-Field and Beyond. *Prog. Part. Nucl. Phys.* **2011**, *66*, 519–548. [CrossRef]
11. Sheikh, J.A.; Dobaczewski, J.; Ring, P.; Robledo, L.M.; Yannouleas, C. Symmetry restoration in mean-field approaches. *J. Phys. G* **2021**, *48*, 123001. [CrossRef]
12. Liu, L.; Otsuka, T.; Shimizu, N.; Utsuno, Y.; Roth, R. No-core Monte Carlo shell-model calculation for ^{10}Be and ^{12}Be low-lying spectra. *Phys. Rev. C* **2012**, *86*, 014302. [CrossRef]
13. Yao, J.M.; Engel, J.; Wang, L.J.; Jiao, C.F.; Hergert, H. Generator-coordinate reference states for spectra and $0\nu\beta\beta$ decay in the in-medium similarity renormalization group. *Phys. Rev. C* **2018**, *98*, 054311. [CrossRef]
14. Yao, J.M.; Bally, B.; Engel, J.; Wirth, R.; Rodríguez, T.R.; Hergert, H. Ab Initio Treatment of Collective Correlations and the Neutrinoless Double Beta Decay of ^{48}Ca. *Phys. Rev. Lett.* **2020**, *124*, 232501. [CrossRef]
15. Frosini, M.; Duguet, T.; Ebran, J.P.; Somà, V. Multi-reference many-body perturbation theory for nuclei: I. Novel PGCM-PT formalism. *Eur. Phys. J. A* **2022**, *58*, 62. [CrossRef]
16. Frosini, M.; Duguet, T.; Ebran, J.P.; Bally, B.; Mongelli, T.; Rodríguez, T.R.; Roth, R.; Somà, V. Multi-reference many-body perturbation theory for nuclei: II. Ab initio study of neon isotopes via PGCM and IM-NCSM calculations. *Eur. Phys. J. A* **2022**, *58*, 63. [CrossRef]
17. Frosini, M.; Duguet, T.; Ebran, J.P.; Bally, B.; Hergert, H.; Rodríguez, T.R.; Roth, R.; Yao, J.; Somà, V. Multi-reference many-body perturbation theory for nuclei: III. Ab initio calculations at second order in PGCM-PT. *Eur. Phys. J. A* **2022**, *58*, 64. [CrossRef]
18. Kimura, M. The Intruder feature of Mg-31 and the coexistence of many particle and many hole states. *Phys. Rev. C* **2007**, *75*, 041302. [CrossRef]
19. Kimura, M. Spectroscopy and intruder configurations of ^{33}Mg and ^{31}Ne studied with antisymmetrized molecular dynamics. *arXiv* **2011**, arXiv:1105.3281.
20. Bally, B.; Avez, B.; Bender, M.; Heenen, P.H. Beyond Mean-Field Calculations for Odd-Mass Nuclei. *Phys. Rev. Lett.* **2014**, *113*, 162501. [CrossRef]

21. Bally, B.; Giacalone, G.; Bender, M. Structure of ^{128,129,130}Xe through multi-reference energy density functional calculations. *Eur. Phys. J. A* **2022**, *58*, 187. [CrossRef]
22. Bally, B.; Giacalone, G.; Bender, M. The shape of gold. *Eur. Phys. J. A* **2023**, *59*, 58. [CrossRef]
23. Borrajo, M.; Egido, J.L. A symmetry-conserving description of odd nuclei with the Gogny force. *Eur. Phys. J. A* **2016**, *52*, 277; Erratum in *Eur. Phys. J. A* **2017**, *53*, 38. [CrossRef]
24. Borrajo, M.; Egido, J.L. Ground-state properties of even and odd Magnesium isotopes in a symmetry-conserving approach. *Phys. Lett. B* **2017**, *764*, 328–334. [CrossRef]
25. Borrajo, M.; Egido, J.L. Symmetry Conserving Configuration Mixing description of odd mass nuclei. *Phys. Rev. C* **2018**, *98*, 044317. [CrossRef]
26. Zhou, E.F.; Wu, X.Y.; Yao, J.M. Multireference covariant density-functional theory for the low-lying states of odd-mass nuclei. *Phys. Rev. C* **2024**, *109*, 034305. [CrossRef]
27. Anguiano, M.; Egido, J.L.; Robledo, L.M. Particle number projection with effective forces. *Nucl. Phys. A* **2001**, *696*, 467–493. [CrossRef]
28. Bender, M.; Duguet, T.; Lacroix, D. Particle-number restoration within the energy density functional formalism. *Phys. Rev. C* **2009**, *79*, 044319. [CrossRef]
29. Duguet, T.; Bender, M.; Bennaceur, K.; Lacroix, D.; Lesinski, T. Particle-number restoration within the energy density functional formalism: Nonviability of terms depending on noninteger powers of the density matrices. *Phys. Rev. C* **2009**, *79*, 044320. [CrossRef]
30. Hergert, H. In-Medium Similarity Renormalization Group for Closed and Open-Shell Nuclei. *Phys. Scr.* **2017**, *92*, 023002. [CrossRef]
31. Egido, J.L.; Lessing, J.; Martin, V.; Robledo, L.M. On the solution of the Hartree-Fock-Bogoliubov equations by the conjugate gradient method. *Nucl. Phys. A* **1995**, *594*, 70–86. [CrossRef]
32. Bally, B.; Sánchez-Fernández, A.; Rodríguez, T.R. Symmetry-projected variational calculations with the numerical suite TAURUS: I. Variation after particle-number projection. *Eur. Phys. J. A* **2021**, *57*, 69; Erratum in *Eur. Phys. J. A* **2021**, *57*, 124. [CrossRef]
33. Yao, J.M.; Meng, J.; Ring, P.; Vretenar, D. Configuration mixing of angular-momentum projected triaxial relativistic mean-field wave functions. *Phys. Rev. C* **2010**, *81*, 044311. [CrossRef]
34. Balian, R.; Brezin, E. Nonunitary bogoliubov transformations and extension of wick's theorem. *Nuovo Cim. B* **1969**, *64*, 37–55. [CrossRef]
35. Pandya, S.P. Nucleon-Hole Interaction in jj Coupling. *Phys. Rev.* **1956**, *103*, 956–957. [CrossRef]
36. Bertsch, G.F.; Robledo, L.M. Symmetry restoration in Hartree-Fock-Bogoliubov based theories. *Phys. Rev. Lett.* **2012**, *108*, 042505. [CrossRef] [PubMed]
37. Avez, B.; Bender, M. Evaluation of overlaps between arbitrary fermionic quasiparticle vacua. *Phys. Rev. C* **2012**, *85*, 034325. [CrossRef]
38. Entem, D.R.; Machleidt, R. Accurate charge-dependent nucleon-nucleon potential at fourth order of chiral perturbation theory. *Phys. Rev. C* **2003**, *68*, 041001. [CrossRef]
39. Bogner, S.K.; Furnstahl, R.J.; Schwenk, A. From low-momentum interactions to nuclear structure. *Prog. Part. Nucl. Phys.* **2010**, *65*, 94–147. [CrossRef]
40. Hebeler, K.; Bogner, S.K.; Furnstahl, R.J.; Nogga, A.; Schwenk, A. Improved nuclear matter calculations from chiral low-momentum interactions. *Phys. Rev. C* **2011**, *83*, 031301. [CrossRef]
41. Fomenko, V.N. Projection in the occupation-number space and the canonical transformation. *J. Phys. A Gen. Phys.* **1970**, *3*, 8–20. [CrossRef]
42. Hergert, H.; Bogner, S.K.; Morris, T.D.; Schwenk, A.; Tsukiyama, K. The In-Medium Similarity Renormalization Group: A Novel Ab Initio Method for Nuclei. *Phys. Rept.* **2016**, *621*, 165–222. [CrossRef]
43. Firestone, R. Nuclear Data Sheets for A = 21. *Nucl. Data Sheets* **2015**, *127*, 1–68. [CrossRef]